· Article · Advances in Polar Science
doi: 10.13679/j.advps.2018.2.00118 June 2018 Vol. 29 No. 2: 118-134

Metamorphism and zircon U-Pb dating of high-pressure pelitic granulites from glacial moraines in the Grove Mountains, East Antarctica

CHEN Longyao[1*], WANG Wei[2], LIU Xiaochun[1] & ZHAO Yue[1]

[1] Institute of Geomechanics, Chinese Academy of Geological Sciences, Beijing 100081, China;
[2] The Office of Hubei Provincial Poverty Alleviation and Development, Wuhan 430071, China

Received 12 December 2017; accepted 28 March 2018

Abstract The Grove Mountains are an inland continuation of the Prydz Belt in East Antarctica. Detailed metamorphic petrological and zircon U-Pb geochronological studies are performed on the high-pressure (HP) pelitic granulites from glacial moraines in the Grove Mountains. The metamorphic peak mineral assemblage of the HP pelitic granulites is characterized by garnet + kyanite + K-feldspar + biotite + plagioclase + quartz, and the subsequent medium-pressure (MP) granulite facies retrogression is characterized by sillimanite replacing kyanite, the formation of the biolite + sillimanite symplectite in the matrix. These mineral assemblages and their P-T estimates based on the P-T pseudosection constructed in MnNCKFMASHT system define a clockwise P-T path involving metamorphic peak of 11.6–13.6 kbar at 817–834°C followed by a near-isothermal decompression of 6.7–7.5 kbar at 806–828°C, comparable with those of associated HP mafic granulites from glacial moraines in the Grove Mountains. Zircon U-Pb dating, coupled with available metamorphic age data obtained for HP mafic granulites, reveals HP metamorphism occurred at 540–545 Ma. Combining the previous research results, the HP pelitic granulites and contemporary HP mafic granulites were widely distributed in glacial moraines from the Grove Mountains, suggesting at least part of the Grove Subglacial Highlands underwent Pan-Afrian HP granulite facies metamorphism, which provides new evidence for a collisional tectonic setting of the Pan-Afrian Prydz Belt.

Keywords East Antarctica, Prydz Belt, Pan-African, HP pelitic granulite

Citation: Chen L Y, Wang W, Liu X C, et al. Metamorphism and zircon U-Pb dating of high-pressure pelitic granulites from glacial moraines in the Grove Mountains, East Antarctica. Adv Polar Sci, 2018, 29(2): 118-134, doi:10.13679/j.advps.2018.2.00118

1 Introduction

The Prince Charles Mountains (PCM)–Prydz Bay region of East Antarctica was previously considered to be a part of a unified East Gondwana craton since Late Mesproterozoic/ Early Neoproterozoic (i.e. Grenvillian) (Stern, 1994; Dalziel, 1991; Hoffman, 1991; Moores, 1991). As the recognition and confirmation of the Late Neoproterozoic/Cambrian (termed Pan-African) high-grade tectono-thermal event in the Prydz Bay, the Pan-Afrian Prydz Belt has been established and distinguished from the Grenvillian terrane (Fitzsimons et al., 1997; Carson et al., 1996; Hensen and Zhou, 1995; Zhao et al., 1995, 1993, 1992, 1991). However, the absence of evidence for pre-collisional oceanic closure and subduction has led to a heated and ongoing debate about the tectonic nature of the Prydz Belt. There are two viewpoints about the nature of the Prydz Belt: a suture that resulted from the collision between the Indo-Antarctica and Australo-Antarctica continental blocks (e.g., Liu et al., 2013, 2009a, 2009b, 2007a, 2007b, 2006; Grew et al., 2012; Boger, 2011;

*Corresponding author, E-mail: chenlongyao1220@163.com

Kelsey et al., 2008; Meert and Lieberman, 2008; Collins and Pisarevsky, 2005; Harley, 2003; Zhao et al., 2003; Boger et al., 2001; Fitzsimons, 2000; Hensen and Zhou, 1997), or an intraplate reworking belt in response to the collision between East and West Gondwana or to convergent orogeny along the proto-Pacific margin of Gondwana (e.g., Tong et al., 2017, 2014, 2002, 1998; Wang et al., 2013, 2008; Halpin et al., 2012; Mikhalsky et al., 2010; Wilson et al., 2007; Phillips et al., 2006; Yoshida et al., 2003; Wilson et al., 1997; Yoshida, 1995).

The Grove Mountains have been also affected by the Pan-African high-grade tectono-thermal event, considered as an inland continuation of the Pan-Afrian Prydz Belt in East Antarctica (Wang et al., 2016a, 2016b; Liu et al., 2013, 2009b, 2007b, 2006, 2003, 2002; Liu et al., 2002; Boger et al., 2001; Mikhalsky et al., 2001; Zhao et al., 2000). Although many studies has been conducted regarding the bedrock exposure of the Grove Mountains, most of the basement in the Grove Mountains is hidden beneath the ice sheet (Liu et al., 2007b, 2006, 2003, 2002; Liu X H et al., 2003; Mikhalsky et al., 2001a; Zhao et al., 2000). The sparse exposures of bedrock are insufficient to fully characterize the geology of the entire area. Previous studies have concluded that the moraine erratics likely came from the southeastern subglacial bedrock of the Grove Mountains (Wang et al., 2016a, 2016b; Hu et al., 2015; Liu et al., 2009b). Therefore, a number of moraine belts exposed on the glaciers of the Grove Mountains may provide important information about the geologic evolution of the Grove Subglacial Highlands. Liu et al. (2009b) identified a number of Pan-African high-pressure (HP) mafic granulites from glacial moraines in the west of the Gale Escarpment. The P-T evolution of those HP mafic granulites provides direct evidence for a collisional tectonic setting for the Pan-African event near the Grove Mountains.

The HP pelitic rocks are of particular significance in understanding the tectonic setting and processes of the Prydz Belt, because only plate tectonic processes involving subduction and continent–continent collision can bring the sedimentary precursors of pelitic rocks into a lower crustal depth where they experience HP metamorphism (Anderson et al., 2012; Appel and Schenk, 1998). In this contribution, we document the first discovery of HP pelitic granulites from the glacial moraines in the Grove Mountains. Detailed metamorphic petrological and geochronological studies are performed to reconstruct the metamorphic P-T-t path of the HP pelitic granulites. The results of the study, combined with previous metamorphic data obtained from other granulite assemblages in the Prydz Belt, provide new evidence for a collisional tectonic setting of the Pan-Afrian Prydz Belt.

2 Geological background

The PCM–Prydz Bay region is dominated by four Archean/Paleoproterozoic cratonic blocks, a Late Mesoproterozoic Fisher Terrane, a Meso-Neoproterozoic Rayner Complex and a Pan-Afrian Prydz Belt. From north to south, four Archean/Paleoproterozoic blocks are the Vestfold Hills Block and the Rauer Group in the Prydz Bay, the Lambert Terrane in the Mawson Escarpment, and the Ruker Terrane in the southern PCM (Figure 1). Each of these blocks has its own distinct crustal history before the Late Neoproterozoic/Cambrian and they are therefore unlikely to represent the remnants of a single unified craton (Boger, 2011; Harley, 2003). Except for the Vestfold Hills Blocks, all of blocks were reworked by a Pan-Afrian tectonothermal event (Harley et al., 2013; Kelsey et al., 2008, 2007, 2003; Phillips et al., 2007; Tong et al., 2006; Boger and Wilson, 2005; Harley et al., 1998; Kinny et al., 1993).

The Fisher Terrane, exposed in the southern sector of the northern PCM, is characterized by an abundance of 1300–1020 Ma mafic-felsic volcanism and intrusions, with subsequent amphibolite-facies metamorphism at 1020–940 Ma (Mikhalsky et al., 2001b, 1999; Kinny et al., 1997; Beliatsky et al., 1994). The Rayner Complex crops out in the MacRobertson and Kemp lands and contains 1490–1020 Ma mafic-felsic volcanism and intrusions and coeval or younger meta-sedimentary rocks (Liu et al., 2017; Boger et al., 2000). Those rocks underwent regional granulite facies metamorphic and were intruded by widespread charnockitic and granitic magmatism at *ca*. 1000–900 Ma (Liu et al., 2017; Morrissey et al., 2015; Wang et al., 2008; Boger et al., 2000; Carson et al., 2000; Kinny et al., 1997). Greenschist-amphibolite facies metamorphism and pegmatite intrusion at *ca*. 550–500 Ma have been reported in some places (Boger et al., 2002; Carson et al., 2000; Fitzsimons and Thost, 1992; Manton et al., 1992). However, a more recent study suggests that this reworking may also have reached higher temperature grades, with P-T conditions of 800–870°C and 5.5–6.5 kbar (Morrissey et al., 2016).

The Prydz Belt crops out along the Prydz Bay coastline, extends southward along the eastern side of the Amery Ice Shelf, and crosses into the Lambert Terrane and the Grove Mountains (Liu et al., 2014a, 2009a, 2007a; Fitzsimons, 2003; Zhao et al., 2003). The rocks in Prydz Bay and eastern Amery Ice Shelf consist mainly of mafic–felsic composite orthogneisses and migmatitic paragneisses, which are considered to be basement and cover sequences, respectively (Liu et al., 2014a, 2009a, 2007a; Grew et al., 2012; Fitzsimons, 1997; Carson et al., 1995; Fitzsimons and Harley, 1991). Geochronological studies suggest that the basement orthogneisses were originally emplaced during the period 1380 to 1020 Ma (Liu et al., 2014a, 2009a, 2007a; Grew et al., 2012; Wang et al., 2008; Zhao et al., 2003, 1995; Sheraton et al., 1984), while the cover sequences might have been deposited during the Late Mesoproterozoic (Grew et al., 2012; Wang et al., 2008; Dirks and Wilson, 1995) or Neoproterozoic (Kelsey et al., 2008; Hensen and Zhou, 1995; Zhao et al., 1995). Most investigators have concluded that two major high-grade metamorphic events affected the eastern Amery Ice Shelf–Prydz Bay area: one at *ca*. 990–900 Ma and

another at *ca*. 530 Ma (e.g., Tong et al., 2014; Liu et al., 2013, 2009a; Wang et al., 2008; Hensen and Zhou, 1995).

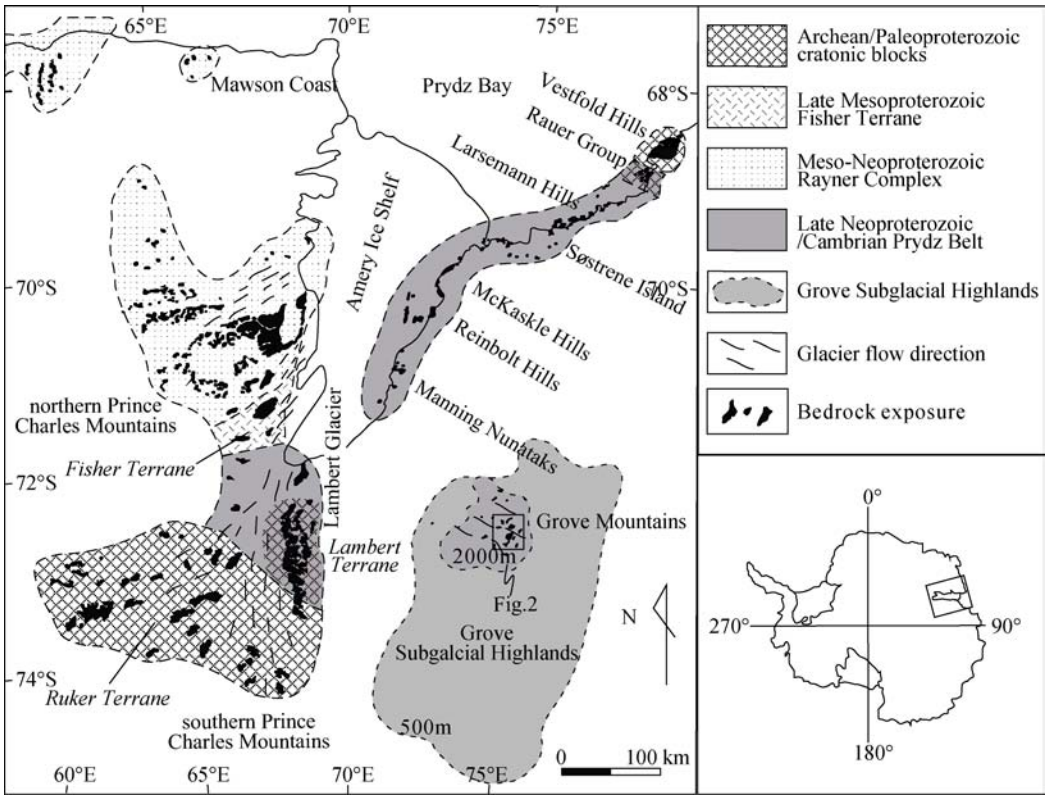

Figure 1 Geological sketch map of the PCM–Prydz Bay region and its location in East Antarctica (modified after Liu et al. (2016), Fitzsimons (2003), Mikhalsky et al. (2001)). The Grove Subglacial Highlands are outlined by the 500-m and 2000-m elevation contours.

The Grove Mountains, located east of the southern PCM, are considered an important part of the Prydz Belt in East Antarctica (Figure 1) (Liu et al., 2009b, 2007b, 2006; Zhao et al., 2003, 2000; Mikhalsky et al., 2001a). This area consists mainly of high-grade metamorphic rocks and abundant charnockites and granites (Liu et al., 2006). The metamorphic rocks are dominated by orthopyroxene-bearing orthogneisses and mafic granulites, with minor garnet-bearing paragneisses and calc-silicate rocks (Liu et al., 2003, 2002). The protoliths of the orthogneisses and mafic granulites formed at *ca*. 920–910 Ma, then experienced Pan-African metamorphism at *ca*. 550–535 Ma (Liu et al., 2007b). The charnockites and granites were emplaced at 547–501 Ma (Liu et al., 2006). The glacial moraine belts occur mainly on glaciers in the area near Mason Peaks, Wilson Ridge, Mount Harding, and Gale Escarpment (Figure 2). All glacial moraines have different distribution characteristics and rock types. The glacial moraines are mainly made up of high-grade metamorphic rocks and granitoids, with minor volcanics and siltstones. Among them, the high-grade metamorphic rocks contain orthogneisses, mafic granulites, HP mafic-pelitic granulites, quartzites, amphibolites, garnet-mica schists and minor calc-silicate rocks (Hu et al., 2016, 2008; Wang et al., 2016a, 2016b). Liu et al. (2009b) identified a number of Pan-African HP mafic granulites from glacial moraines in the west of the Gale Escarpment. The P-T path calculated for the HP mafic granulites involved peak metamorphic conditions of 11.8–14.0 kbar and 770–840°C, and a subsequent near-isothermal decompression of 6 kbar. These data provide direct evidence for a collisional tectonic setting for the Pan-African high-grade metamorphic event in the Grove Mountains.

3 Samples and analytical techniques

HP pelitic granulites were collected as moraine erratics from glacial moraine belts in the Mason Peaks and the northern Gale Escarpment and their locations are shown in Figure 2. In order to constrain the P-T-t path of the those rocks, two HP pelitic granulites (samples GR14-3-18 and GR14-15-7) were selected for detailed petrological study and laser ablation inductively coupled plasma mass spectrometry (LA-ICP-MS) U-Pb zircon analyses.

Mineral compositions were analyzed using a JEOL JXA-8100 electron microprobe (EMP) at the MLR Key Laboratory of Metallogeny and Mineral Assessment, Institute of Mineral Resources, Chinese Academy of Geological Sciences. The operating conditions were 15 kV accelerating voltage, a 10 nA beam current and a counting time of 10 s for each peak. The beam diameter was set to 2 μm for all minerals. Well-defined natural minerals were used as

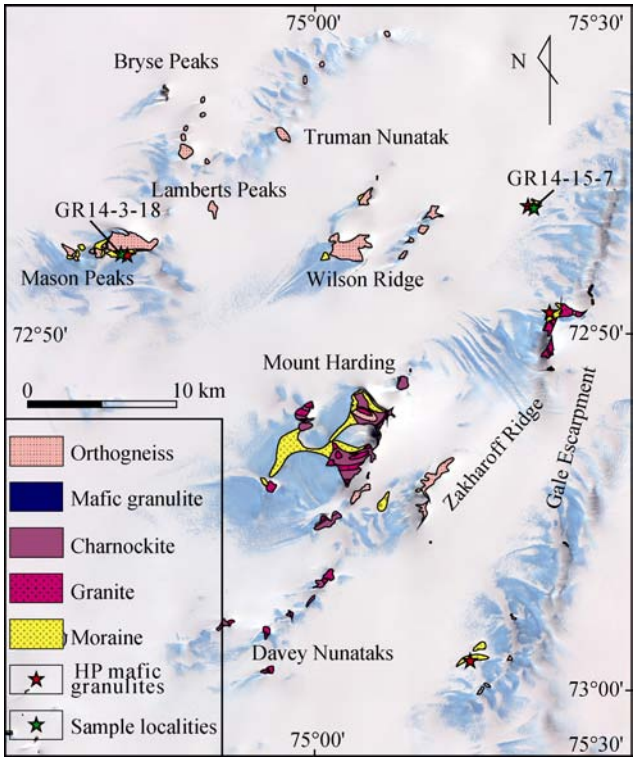

Figure 2 Geologic map of the Grove Mountains superimposed on a remote sensing image. Sampling localities of HP pelitic granulites used in this study are indicated by green stars. Sampling localities of HP mafic granulites are from Wang et al. (2016), Liu et al. (2009b).

standards. Ferric iron in garnet was determined by charge balance. Ferric iron in biotite was estimated based on the assumption of $Fe^{3+}/(Fe^{2+} + Fe^{3+}) = 0.116$ (Holdaway et al., 1997). Representative mineral analyses are presented in Table 1. Whole-rock chemical analyses were carried out at the National Research Center for Geoanalysis, Chinese Academy of Geological Sciences. Major element abundances, except for FeO which was determined by a wet chemical method, were measured by XRF (3080E) after fusion of sample powder with lithium tetraborate. Relative standard deviations are better than 5%.

Zircon U-Pb dating and trace element analyses of zircon were conducted synchronously by LA-ICP-MS at the State Key Laboratory of Geological Processes and Mineral Resources, China University of Geosciences, Wuhan, China, following the procedure described by Hu et al. (2008) and Liu et al. (2010). During the analyses, the output energy was set to 60 mJ, with a pulse repetition rate of 8 Hz and a 32 μm diameter laser spot size for the zircon cores and rims. For U, Th, Pb, and other trace element analyses, calibration used the NIST610 reference glass and ^{29}Si as an internal standard, as well as working values recommended by Pearce et al. (1996). The average analytical error ranged from ±10% for light rare earth elements (LREE) to ±5% for other rare earth elements (REE). Isotopic ratios were calculated using ICPMSDataCal 8.0 (Liu et al., 2010), then corrected for both instrumental mass bias and depth-dependent elemental and isotopic fractionation using Harvard zircon 91500 as an external standard. Ages were obtained using the software package ISOPLOT 3.23 (Ludwig, 2003). The age uncertainties for individual analyses are one standard deviation (1σ), and the calculated weighted mean ages are quoted at the 95% (2σ) confidence level. Trace element compositions of zircons were calibrated against multiple- reference materials (BCR-2G and BIR-1G) combined with internal standardization. The analytical data of isotopes and trace elements are listed in Table 2 and Table 3, respectively.

4 Metamorphic geology

4.1 Petrography

Sample GR14-3-18 is representative of HP pelitic granulites collected from glacial moraine belts in the Mason Peaks. The sample was mainly composed of garnet, kyanite, K-feldspar, plagioclase, biotite and quartz (Figures 3a, 3b). Accessory minerals are rutile, ilmenite, monazite and zircon. Garnets occur as idiomorphic to hypidiomorphic porphroblasts, and commonly show corroded morphology with size of 0.8–7.5 mm in diameter. The mineral inclusions show zoned patterns: (1) an inclusion-rich core with abundant fine-grained quartz, (2) a diablastic mantle with coarse-grain quartz, rare biotite and minor accessory minerals of monazite, and (3) an inclusion-rare rim (Figures 3c, 3d). Kyanite occurs as small fragmentary crystals, coexisting with rutile and biotite. Notably, all kyanite grains are surrounded by the coronas of plagioclase, representing the decompressional reaction (Gr+Als+Qz = An) (Figures 3a, 3c). The coronas separate the kyanite from K-feldspar and quartz. Biotite and rutile appear mainly with garnet and kyanite. Plagioclase occurs mainly as platy crystals in contact with garnet, or is intergrown with biotite around kyanite, indicative of decompression retrogression. K-feldspar occurs as large, anhedral perthite in the matrix. Therefore, the representative mineral assemblage of the peak metamorphic stage is garnet, kyanite, plagioclase, K-feldspar, biotite, quartz, rutile and melt.

Sample GR14-15-7 is a sillimanite-bearing pelitic granulite collected from glacial moraine belts in the northern Gale Escarpment. It contains predominately garnet, sillimanite, K-feldspar, plagioclase, biotite and quartz. Accessory minerals are rutile, ilmenite, apatite and zircon. The garnet grains, typically 1–8 mm across, occur as porphyroblasts with cores containing inclusions of quartz, biotite, plagioclase, kyanite and minor accessory minerals of zircon, whereas the rims contain significantly fewer inclusions of quartz and sillimanite than the cores (Figures 3e, 3f). Biotite and plagioclase appear mainly in three textural domains, the first type is included in garnet grains, the second type is discrete flakes in matrix, and the third type is as symplectite of biotite + plagioclase around garnet, indicative

Table 1 Representative microprobe analyses of minerals for HP pelitic granulites from the Grove Mountains

Sample	GR14-3-18			GR14-15-7			GR14-3-18				GR14-15-7			
Min	Grt	Grt	Grt	Grt	Grt	Grt	Bt	Bt	Pl	Pl	Bt	Bt	Pl	Pl
Loc	rim	mantle	core	rim	mantle	core	incl.	matrix	matrix	matrix	incl.	matrix	matrix	matrix
SiO_2	38.16	37.94	37.74	36.89	37.12	36.88	37.46	36.75	59.56	60.30	35.47	35.46	61.53	61.32
TiO_2	0.04	0.05	0.03	0.04	0.05	0.00	1.58	2.44	0.03	0.00	1.31	1.68	0.00	0.00
Al_2O_3	21.62	21.37	21.37	20.84	20.99	20.98	18.16	18.16	24.25	24.02	17.72	17.79	23.67	23.41
Cr_2O_3	0.16	0.07	0.03	0.02	0.06	0.00	0.40	0.82	0.03	0.01	0.10	0.07	0.00	0.00
FeO	28.61	28.04	28.20	34.42	33.20	32.11	12.97	13.29	0.04	0.02	18.50	19.44	0.00	0.02
MgO	8.18	8.02	8.01	4.60	5.84	6.06	13.52	11.61	0.00	0.00	9.33	8.95	0.00	0.00
MnO	0.70	0.78	0.75	0.36	0.28	0.21	0.00	0.00	0.00	0.02	0.06	0.00	0.01	0.03
CaO	2.63	2.98	2.97	1.27	1.41	1.44	0.00	0.00	7.63	6.80	0.00	0.00	5.81	5.83
Na_2O	0.00	0.01	0.02	0.00	0.01	0.00	0.08	0.08	7.93	7.94	0.10	0.10	8.63	8.62
K_2O	0.01	0.00	0.00	0.00	0.00	0.00	9.05	9.68	0.14	0.24	9.58	9.70	0.07	0.12
Total	100.1	99.3	99.1	98.4	99.0	97.7	93.22	92.83	99.62	99.36	92.17	93.18	99.71	99.36
O	12.0	12.0	12.0	12.0	12.0	12.0	11.0	11.0	8.0	8.0	11.0	11.0	8.0	8.0
Si	2.95	2.96	2.95	2.99	2.96	2.97	2.81	2.79	2.66	2.70	2.79	2.77	2.74	2.74
Al	1.97	1.97	1.97	1.99	1.98	1.99	1.60	1.62	1.28	1.27	1.64	1.64	1.24	1.23
Ti	0.00	0.00	0.00	0.00	0.00	0.00	0.09	0.14	0.00	0.00	0.08	0.10	0.00	0.00
Fe^{3+}	0.11	0.10	0.13	0.03	0.09	0.06	0.00	0.00	0.00	0.00	0.00	0.00	0.00	0.00
Cr	0.01	0.00	0.00	0.00	0.00	0.00	0.02	0.05	0.00	0.00	0.01	0.00	0.00	0.00
Mg	0.94	0.93	0.93	0.56	0.69	0.73	1.51	1.31	0.00	0.00	1.09	1.04	0.00	0.00
Fe^{2+}	1.74	1.73	1.71	2.30	2.13	2.11	0.81	0.84	0.00	0.00	1.22	1.27	0.00	0.00
Mn	0.05	0.05	0.05	0.02	0.02	0.01	0.00	0.00	0.00	0.00	0.00	0.00	0.00	0.00
Ca	0.22	0.25	0.25	0.11	0.12	0.12	0.00	0.00	0.36	0.33	0.00	0.00	0.28	0.28
Na	0.00	0.00	0.00	0.00	0.00	0.00	0.01	0.01	0.69	0.69	0.01	0.01	0.74	0.75
K	0.00	0.00	0.00	0.00	0.00	0.00	0.87	0.94	0.01	0.01	0.96	0.97	0.00	0.01
$Mg^{\#}$	0.351	0.351	0.353	0.194	0.246	0.257	7.73	7.71	5.00	5.00	7.80	7.80	5.00	5.00
X_{Mg}	0.320	0.315	0.317	0.186	0.234	0.245	0.650	0.609			0.473	0.451		
X_{Fe}^{2+}	0.591	0.583	0.582	0.769	0.719	0.708			0.344	0.317			0.270	0.270
X_{Mn}	0.016	0.017	0.017	0.008	0.006	0.005			0.648	0.670			0.726	0.723
X_{Ca}	0.074	0.084	0.085	0.037	0.041	0.042			0.008	0.013			0.004	0.007

Table 2 LA-ICP-MS U-Pb analyses for zircons from HP pelitic granulites from the Grove Mountains

Spot	Th /ppm	U /ppm	Th/U	Isotopic ratios						Ages /Ma						Concordance
				$^{207}Pb/^{206}Pb$	$\pm\sigma$	$^{207}Pb/^{235}U$	$\pm\sigma$	$^{206}Pb/^{238}U$	$\pm\sigma$	$^{207}Pb/^{206}Pb$	$\pm\sigma$	$^{207}Pb/^{235}U$	$\pm\sigma$	$^{206}Pb/^{238}U$	$\pm\sigma$	
Sample GR14-3-18																
1	31.0	1690	0.018	0.0572	0.0010	0.6264	0.0112	0.0790	0.0007	502	39	494	7.0	490	4.1	99%
2	16.3	1119	0.015	0.0584	0.0011	0.6648	0.0134	0.0822	0.0008	546	38.9	518	8.2	509	5.0	98%
3	13.4	1035	0.013	0.0569	0.0010	0.6270	0.0127	0.0796	0.0008	487	36.1	494	7.9	494	4.6	99%
4	11.4	486	0.024	0.0591	0.0030	0.7184	0.0374	0.0880	0.0012	572	112.9	550	22.1	543	7.2	98%
5	17.8	1182	0.015	0.0691	0.0015	0.8375	0.0207	0.0870	0.0007	902	44.4	618	11.5	538	4.2	86%
6	12.2	1856	0.007	0.1495	0.0019	4.8702	0.0776	0.2350	0.0026	2340	21.9	1797	13.5	1361	13.6	72%
7	10.8	1474	0.007	0.1604	0.0021	6.8335	0.1476	0.3069	0.0051	2461	22.2	2090	19.2	1725	25.0	80%

Continued

Spot	Th /ppm	U /ppm	Th/U	Isotopic ratios						Ages /Ma						Concordance
				$^{207}Pb/^{206}Pb$	$\pm\sigma$	$^{207}Pb/^{235}U$	$\pm\sigma$	$^{206}Pb/^{238}U$	$\pm\sigma$	$^{207}Pb/^{206}Pb$	$\pm\sigma$	$^{207}Pb/^{235}U$	$\pm\sigma$	$^{206}Pb/^{238}U$	$\pm\sigma$	
Sample GR14-3-18																
8	13.7	886	0.015	0.0704	0.0017	0.7994	0.0188	0.0820	0.0009	943	44.3	596	10.6	508	5.3	84%
9	12.4	752	0.016	0.0605	0.0012	0.7294	0.0137	0.0872	0.0008	620	38.0	556	8.0	539	4.8	96%
10	16.1	1420	0.011	0.0809	0.0022	0.9218	0.0293	0.0819	0.0009	1220	53.7	663	15.5	507	5.4	73%
11	10.1	916	0.011	0.1631	0.0022	5.8413	0.1038	0.2583	0.0030	2488	22.8	1953	15.5	1481	15.2	72%
12	13.3	970	0.014	0.0610	0.0012	0.7407	0.0147	0.0878	0.0009	639	40.7	563	8.6	542	5.4	96%
13	13.3	814	0.016	0.0612	0.0018	0.6864	0.0185	0.0814	0.0010	656	63.0	531	11.1	505	6.1	94%
14	14.8	1102	0.013	0.0622	0.0011	0.7024	0.0127	0.0817	0.0007	681	30.6	540	7.6	507	4.0	93%
15	22.5	1165	0.019	0.0611	0.0017	0.7264	0.0188	0.0866	0.0010	643	57.2	554	11.1	535	5.8	96%
16	11.1	1278	0.009	0.1619	0.0026	6.2645	0.1669	0.2796	0.0051	2476	26.7	2013	23.4	1589	26.0	76%
17	16.3	995	0.016	0.0613	0.0013	0.6189	0.0171	0.0731	0.0012	650	44.4	489	10.7	455	7.1	92%
18	14.0	1030	0.014	0.0896	0.0072	1.0700	0.1642	0.0839	0.0066	1418	154	739	80.6	520	39.0	65%
19	18.5	399	0.047	0.0651	0.0019	0.6704	0.0192	0.0749	0.0007	776	57.2	521	11.7	465	4.5	88%
20	20.3	421	0.048	0.1247	0.0047	1.5335	0.0671	0.0879	0.0010	2025	61.9	944	26.9	543	6.1	46%
21	12.1	508	0.024	0.0816	0.0027	0.9046	0.0313	0.0802	0.0008	1236	64.5	654	16.7	497	5.1	72%
22	15.2	1186	0.013	0.0646	0.0012	0.7926	0.0245	0.0873	0.0013	761	240	593	13.9	540	8.0	90%
23	14.8	857	0.017	0.1458	0.0021	3.5793	0.0670	0.1772	0.0019	2298	24.7	1545	14.9	1051	10.2	61%
24	10.5	703	0.015	0.0588	0.0012	0.6597	0.0131	0.0812	0.0007	567	47.2	514	8.0	503	4.3	97%
Sample GR14-15-7																
1	9.41	924	0.010	0.0617	0.0019	0.7430	0.0231	0.0883	0.0018	661	66.7	564	13.5	545	10.6	96%
2	62.5	1759	0.036	0.0670	0.0021	0.8299	0.0477	0.0881	0.0035	839	64.8	614	26.5	544	20.9	88%
3	21.4	2120	0.010	0.0583	0.0015	0.7114	0.0245	0.0883	0.0022	543	55.5	546	14.6	545	12.9	99%
4	51.1	938	0.054	0.0863	0.0041	1.0366	0.0531	0.0872	0.0024	1346	90.7	722	26.5	539	14.0	70%
5	59.7	1385	0.043	0.0565	0.0017	0.6825	0.0246	0.0871	0.0015	478	97.2	528	14.8	538	9.0	98%
6	43.8	2209	0.020	0.0705	0.0016	0.8785	0.0259	0.0896	0.0015	943	48	640	14.0	553	9.1	85%
7	48.0	737	0.065	0.0566	0.0017	0.6918	0.0244	0.0882	0.0016	480	66.7	534	14.6	545	9.6	97%
8	85.5	2048	0.042	0.0577	0.0021	0.7002	0.0252	0.0879	0.0014	520	81.5	539	15.1	543	8.5	99%
9	9.02	710	0.013	0.0786	0.0036	1.0072	0.0685	0.0887	0.0026	1163	60.2	707	34.6	548	15.6	74%
10	21.2	2477	0.009	0.0603	0.0016	0.7372	0.0261	0.0877	0.0019	617	52.8	561	15.2	542	11.3	96%
11	13.6	642	0.021	0.0889	0.0049	1.0468	0.0474	0.0883	0.0015	1411	102	727	23.5	546	8.7	71%
12	18.8	584	0.032	0.0613	0.0018	0.7471	0.0239	0.0883	0.0016	650	69.4	567	13.9	545	9.6	96%
13	12.9	894	0.014	0.0576	0.0016	0.6768	0.0212	0.0843	0.0012	522	59.3	525	12.8	522	7.3	99%
14	24.7	3174	0.008	0.0648	0.0019	0.8033	0.0340	0.0878	0.0017	769	63.0	599	19.2	543	9.9	90%
15	20.4	2391	0.009	0.0577	0.0015	0.7078	0.0184	0.0886	0.0014	517	55.6	543	10.9	547	8.0	99%

Table 3 Trace element compositions (in ppm) of zircons from HP pelitic granulites from the Grove Mountains

Spot	La /ppm	Ce /ppm	Pr /ppm	Nd /ppm	Sm /ppm	Eu /ppm	Gd /ppm	Tb /ppm	Dy /ppm	Ho /ppm	Er /ppm	Tm /ppm	Yb /ppm	Lu /ppm
Sample GR14-3-18														
1	0.181	4.45	0.178	2.02	3.13	1.93	7.38	1.22	8.46	1.63	4.44	0.676	4.99	0.654
2	0.093	2.58	0.124	1.16	1.79	0.994	4.02	0.667	4.44	0.744	1.85	0.260	1.89	0.273
3	0.038	1.81	0.068	0.903	1.70	0.923	3.77	0.674	4.27	0.752	1.97	0.265	1.71	0.246
4	0.128	2.63	0.105	0.734	1.32	0.800	2.33	0.576	4.71	0.983	2.93	0.388	3.16	0.445
5	0.630	9.73	0.589	4.04	3.21	3.09	5.52	0.881	6.53	1.22	3.17	0.467	3.59	0.502
6	0.877	10.8	0.854	5.72	3.83	3.04	9.83	2.16	15.7	2.68	6.90	1.04	8.55	1.138
7	0.947	8.55	1.03	6.62	4.31	3.33	10.6	2.40	17.4	3.20	8.30	1.26	10.1	1.460
8	0.143	2.19	0.129	1.25	1.37	1.01	2.86	0.515	3.35	0.663	1.78	0.253	1.73	0.225
9	0.003	1.15	0.025	0.559	1.44	0.683	3.69	0.631	3.78	0.640	1.57	0.187	1.26	0.162
10	0.194	3.16	0.212	1.60	1.42	1.12	2.92	0.468	3.27	0.638	1.74	0.270	1.70	0.221
11	0.559	5.49	0.387	2.27	1.58	1.66	4.52	1.01	7.66	1.52	4.79	0.903	8.62	1.39
12	0.006	1.36	0.034	0.75	2.19	0.991	5.73	0.948	6.07	0.995	2.41	0.318	2.22	0.311
13	0.028	1.50	0.049	0.905	2.05	1.05	4.27	0.604	4.20	0.743	1.84	0.284	2.02	0.242
14	0.137	2.76	0.149	1.55	2.18	1.60	4.64	0.740	4.62	0.897	2.23	0.317	2.13	0.324
15	0.168	3.99	0.181	2.18	3.17	2.12	7.28	1.23	9.66	1.92	6.47	0.914	6.43	0.952
16	1.36	15.4	1.69	10.2	4.70	4.72	9.10	2.19	17.9	3.52	9.29	1.50	11.4	1.70
17	0.070	2.43	0.115	1.21	1.66	0.869	3.63	0.591	3.93	0.708	1.81	0.287	1.87	0.270
18	0.143	2.35	0.158	1.23	1.42	1.10	3.48	0.530	4.50	0.775	2.22	0.438	3.22	0.373
19	0.031	1.94	0.078	1.40	2.55	0.825	5.89	1.01	6.26	1.16	2.78	0.438	2.95	0.387
20	0.519	5.54	0.393	3.61	3.09	2.51	5.69	1.02	8.08	1.59	4.16	0.565	3.91	0.522
21	0.169	2.17	0.132	1.21	1.62	1.06	4.45	0.741	5.21	1.00	2.52	0.369	2.48	0.366
22	0.105	2.71	0.129	1.34	1.73	1.10	3.99	0.629	4.05	0.697	1.73	0.239	1.61	0.228
23	0.060	1.97	0.093	0.872	1.33	0.651	3.78	0.764	6.57	1.59	6.31	1.37	14.6	2.965
24	0.038	1.78	0.073	0.775	1.23	0.739	2.96	0.539	3.51	0.646	1.66	0.213	1.58	0.198
Sample GR14-15-7														
1	0.017	0.237	0.012	0.058	0.735	0.153	9.70	4.43	63.0	12.3	43.5	6.03	53.2	6.65
2	0.541	3.76	0.367	1.47	0.820	0.459	5.17	1.70	24.7	5.47	28.1	5.52	65.6	10.5
3	0.020	0.552	0.011	0.126	0.340	0.223	5.22	1.53	20.5	3.50	12.8	1.68	17.5	2.32
4	0.065	0.851	0.046	0.500	1.39	0.194	11.0	3.78	49.5	9.63	31.1	4.29	40.2	5.00
5	0.104	0.632	0.036	0.479	1.81	0.283	11.1	2.33	22.0	2.63	6.96	0.732	5.64	0.571
6	1.67	14.2	1.95	12.4	5.03	5.09	13.7	3.72	50.7	9.84	42.3	7.17	76.7	12.9
7	0.019	0.571	0.029	0.366	1.08	0.125	9.55	2.43	25.8	3.98	11.1	1.45	12.0	1.40
8	0.833	7.63	0.606	4.25	2.16	1.58	6.90	1.64	19.9	4.89	20.6	4.04	49.3	7.52
9	0.705	3.92	0.306	2.15	1.62	1.28	12.2	4.27	59.6	11.6	39.9	5.64	47.4	6.26
10	1.10	10.00	1.27	7.50	3.07	3.20	8.31	1.50	16.7	2.81	9.58	1.39	12.9	1.66
11	0.626	4.76	0.581	3.77	2.08	1.39	9.58	3.50	53.7	11.4	42.9	6.20	59.5	8.08
12	0.024	0.335	0.003	0.176	0.78	0.157	6.72	2.68	34.6	6.35	21.7	3.14	28.5	3.50
13	0.068	0.387	0.022	0.166	0.727	0.162	9.69	4.22	62.3	12.5	44.7	6.21	57.8	7.07
14	0.918	8.67	0.523	3.19	1.60	1.47	8.74	2.21	29.1	5.80	21.6	3.44	32.0	4.14
15	0.057	0.959	0.080	0.377	0.591	0.523	5.88	1.72	18.6	3.10	10.2	1.37	14.7	1.77

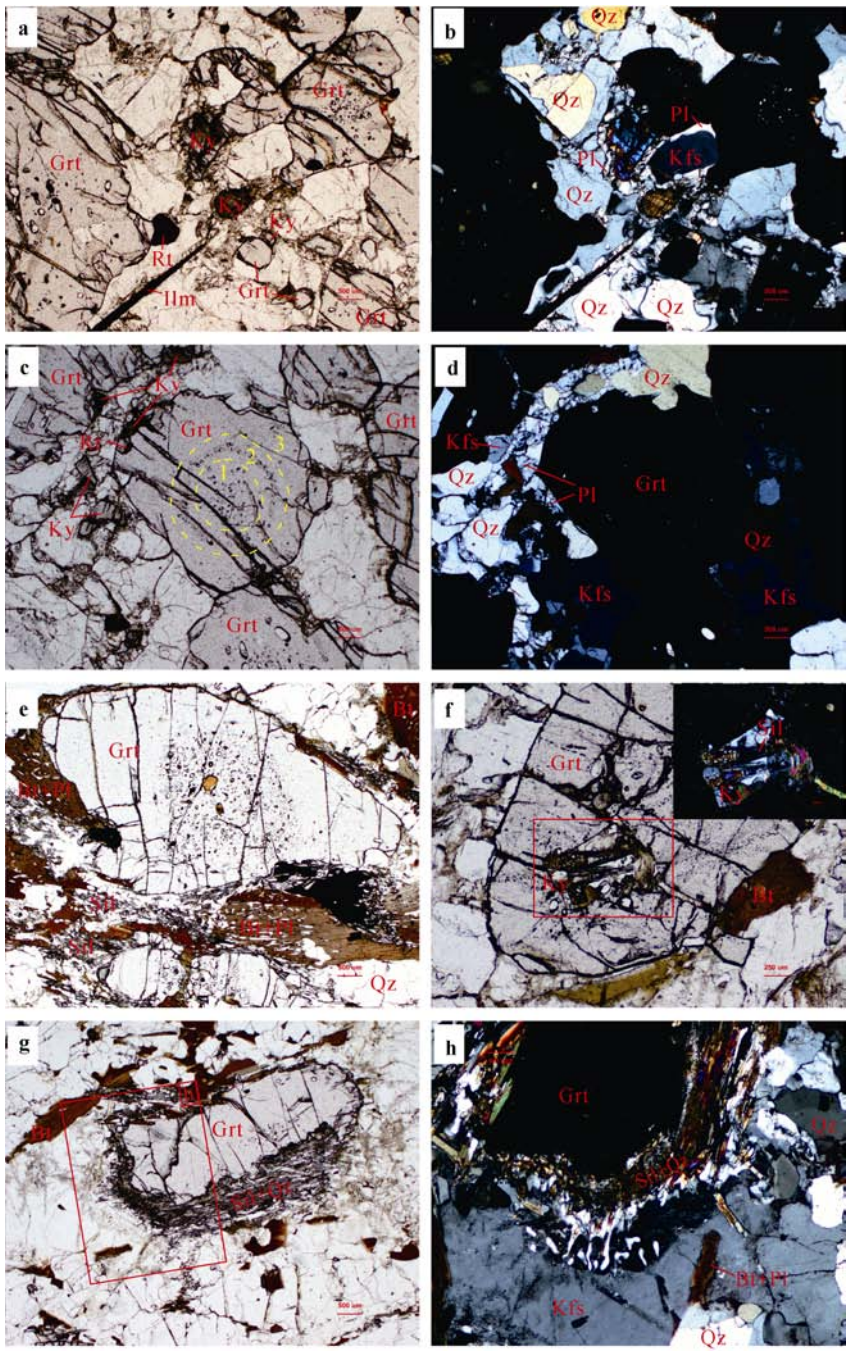

Figure 3 Representative photomicrographs showing the mineral textures and parageneses in HP pelitic granulites from the glacial moraines in the Grove Mountains. **a**–**b**, Kyanites surrounded by the coronas of plagioclase from sample GR14-3-18; **c**–**d**, Garnet with inclusion-zoned pattern from sample GR14-3-18; **e**, The biotite + plagioclase symplectite around garnet from sample GR14-15-7; **f**, Kyanite and the transition from kyanite to sillimanite are preserved in garnet from sample GR14-15-7; **g**–**h**, Sillimanites as aggregates intergrowing with quartz surrounding garnet from sample GR14-15-7. Mineral abbreviations: Bt–biotite, Grt–garnet, Kfs–K-feldspar, Ky–kyanite, Pl–plagioclase, Qz–quartz, Rt–rutile, Sil–sillimanite.

of melting reaction operating in reverse during retrograde metamorphic stages (Figure 3e). Sillimanite can be divided into three groups by occurrence: (1) as aggregates intergrowing with quartz surrounding garnet (Figures 3g, 3h), (2) as acicular inclusions at the rim of large garnet porphyroblasts and some small garnets (Figure 3f), (3) as pesudomorphs of kyanite. Kyanite is only recognized as inclusions within garnet. K-feldspar occurs as large, anhedral perthite in the matrix. Rutile is distributed occasionally around garnet. Ilmenite occurs mainly with biotite and sillimanite around garnet. The representative mineral assemblage of the peak metamorphic stage is garnet mantle

and its inclusions of kyanite, biotite, plagioclase, K-feldspar, quartz, rutile and melt. The post-peak decompression assemblage is characterized by garnet rim, sillimanite, biotite, plagioclase, K-feldspar, quartz, and ilmenite, representing the imprinted MP granulite facies stage.

4.2 Mineral chemistry

Garnet in the sample GR14-3-18 is dominated by almandine (X_{alm} 0.58–0.60), pyrope (X_{py} 0.31–0.33) and grossular (X_{gr} 0.07–0.09), with minor spessartine (X_{spss} 0.01–0.03). Though the analyzed garnets have complex core–mantle–rim texture, they show no siginificant composition zoning from core to near the rim, except for slightly rim-ward increase of almandine and decrease of grossular (Figure 4). The relatively homogenous composition might be derived from compositional homogenization at the peak metamorphic stages, while the decreasing X_{gr} in the rim is consistent with decompression-driven resorption of garnet (e.g., Cooke et al., 2000; Pattison and Begin, 1994; Spear et al., 1993). Garnet in the sample GR14-15-7 is dominated by almandine (X_{alm} 0.71–0.77) and pyrope (X_{py} 0.19–0.24), with minor grossular (X_{gr} 0.02–0.04) and spessartine (X_{spss} <0.01). The core and mantle of the analyzed garnet do not show a pronounced compositional variation, whereas the rim exhibits a significant increase in almandine and spessartine and decrease in pyrope and grossular. This compositional variation indicates a compositional homogenization at the peak metamorphic stages, followed by retrograde re-equilibration.

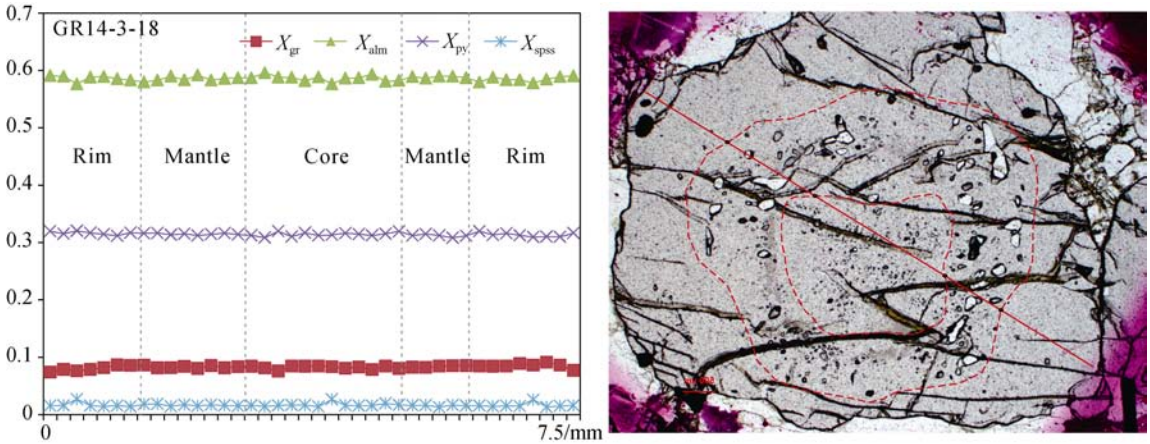

Figure 4 Representative compositional zoning profiles and photomicrographs for garnet from HP pelitic granulite sample GR14-3-18 from the Grove Mountains. The red solid line refers to the location of the garnet compositional zoning profile. Mineral abbreviations: alm–almandine, gr–grossular, py–pyrope, spss–spessartine.

Two types of biotite grains were analyzed according to microstructural observation. Biotites from the two samples have similar compositional characteristic. Biotites contacting with garnets have relatively higher X_{Mg} (0.635–0.657) and lower Ti (0.089–0.115), with increasing Ti from core to rim, while those off garnet in the matrix exhibit lower X_{Mg} (0.608–0.611) and higher Ti (0.111–0.139). The higher X_{Mg} might be attributed to partial or complete re-equilibrium with garnet during retrograde evolution (e.g., Spear and Florence, 1992).

Plagioclases around garnet or intergrowing with biotite around kyanite in the sample GR14-3-18 have homogeneous compositions with An [An = Ca/(Ca+Na+K)] contents of 0.312–0.404, which are classifield as andesine. Some plagioclase grains surrounding kyanite have lower An contents. Plagioclases in the sample GR14-15-7 are oligoclase with An contents of 0.249–0.278.

4.3 P-T pseudosection calculations

Based on the mineral assemblages and compositions for two HP pelitic granulites (sample GR14-3-18 and GR14-15-7), P-T pseudosections were calculated in the MnO–Na_2O–CaO–K_2O–FeO–MgO–Al_2O_3–SiO_2–H_2O–TiO_2 (MnNCKFMASHT) system by using the internally consistent thermodynamic data set of Holland and Powell (1998, updated in 2003) and the PERPLE_X computer program package (Connolly, 2005; version of August 2012). Pseudosection construction considered the following solid-solution models: garnet (White et al., 2007), biotite (Tajčmanovă et al., 2007), cordierite (Holland and Powell, 1998), feldspar (Benisek et al., 2003), muscovite (Coggon and Holland, 2002), paragonite (Coggon and Holland, 2002), chlorite, ilmenite (White et al., 2007), silicate melt (White et al., 2001). Pure phases included water (H_2O), sillimanite (sill), kyanite (ky), andalusite (and) and quartz (q).

The pseudosection was constructed using the measured bulk-rock composition, which represents the final rock composition, if a certain amount of melt was lost during prograde evolution. Therefore, this pseudosection allows the exploration of the phase equilibria in the high-T part of the metamorphic history and the assessment of the near-to-the peak and the retrograde evolution, but may not be valid for the prograde evolution of the rock (Indares et al., 2008; White et al., 2004). The stability field of the peak and retrograde mineral assemblage on the pseudosection are the first-order to constrain the respective metamorphic P-T conditions. The X_{Mg} [=Mg/(Mg+Fe)] and X_{Ca} [=Ca/(Fe+Ca+Mg+Mn)] isopleths in

garnet were used to estimate further information on the P-T evolution of the studied samples.

The P–T pseudosection calculated for sample GR14-3-18 is drawn for garnet, plagioclase and quartz in excess with the P-T window of 4–14 kbar and 700–900°C (Figure 5). The fluid-absent solidus occurs at temperatures between 810°C and 850°C and rutile appears above 6.5 kbar. Cordierite appears below 6.1 kbar and biotite disappears at 820–865°C. The observed peak assemblage Grt + Bt + Ky + Kfs + Pl + Qz + Rt is stable in the P-T range of 810–840°C and 10.5–14.0 kbar (Figure 5). As described above, garnet from sample GR14-3-18 show no significant composition zoning from core to rim (Table 1 and Figure 4). For the garnet core, the composition isopleths of X_{Mg} = 0.315–0.320 and X_{Ca} = 0.084–0.085 intersect at the P-T field of *ca*. 817°C and *ca*. 13.6 kbar (the red circle 1 in Figure 5). For the garnet rim, the composition isopleths of X_{Mg} = 0.320 and X_{Ca} = 0.074–0.075 intersect at the P-T field of *ca*. 834°C and *ca*. 11.6 kbar (the red circle 2 in Figure 5). The garnet core and rim composition isopleths intersect exactly

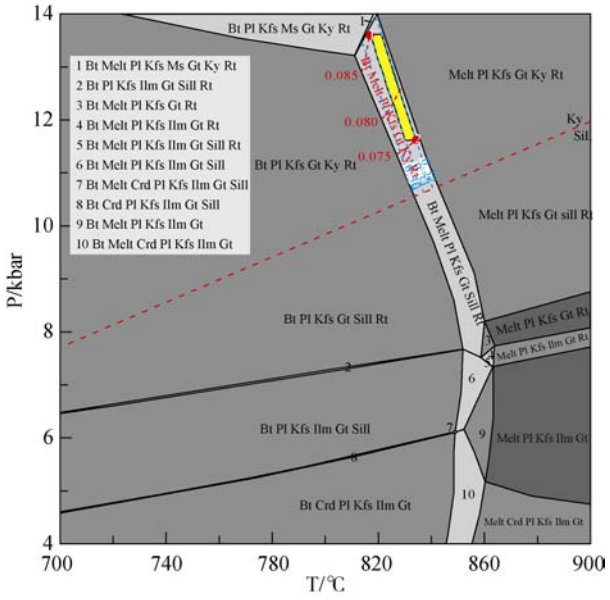

Figure 5 P-T pseudosections based on the bulk-rock compositions (SiO_2 = 59.92, TiO_2 = 0.53, Al_2O_3 = 15.92, FeO = 13.50, MgO = 4.05, MnO = 0.30, CaO = 1.73, Na_2O = 0.71, K_2O = 2.51, and H_2O = 0.21 in wt. %) of the HP pelitic granulite sample GR14-3-18 from the Grove Mountains in the MnNCKFMASHT system. The red bold fonts refer to the observed peak mineral assemblages. The blue and red dashed lines represent isopleths of X_{Mg} and X_{Ca} in garnet, respectively. The semitransparent red circles marked by numbers 1 and 2 refer to the P-T conditions constrained by the garnet core and rim composition isopleths, respectively. The yellow ellipse represents peak metamorphic condition.

at the stability field of the observed peak mineral assemblage (Figure 5). Thus the sample GR14-3-18 underwent peak-stage granulite-facies metamorphism at P-T conditions of 817–834°C and 11.6–13.6 kbar.

The P-T pseudosection calculated for sample GR14-15-7 shows that garnet, plagioclase and quartz are stable in the calculated P-T range of 4–14 kbar and 700–900°C (Figure 6). The fluid-absent solidus occurs at temperatures between 700°C and 725°C and rutile appears above 8.5 kbar. Cordierite appears below 5.0 kbar and biotite disappears at *ca*. 795–835°C. The observed peak assemblage Grt + Bt + Ky + Kfs + Pl + Qz + Rt is stable in the P-T range of *ca*. 9.4–12.6 kbar and *ca*. 770–815°C (the red region in Figure 6). The retrograde assemblage Grt + Bt + Sil + Kfs + Pl + Qz + Rt is stable in the P-T range of ca 780–835°C and *ca*. 5.0–7.0 kbar. For the garnet core, the composition isopleths of X_{Mg} = 0.245 and X_{Ca} = 0.042 intersect at the P-T field of *ca*. 828°C and *ca*. 7.5 kbar, which drops into the stability field of the retrograde mineral assemblage (the red circle 1 in Figure 6). For the garnet rim, the composition isopleths of X_{Mg} = 0.186 and X_{Ca} = 0.037 intersect at the P-T field of *ca*. 806°C and *ca*. 6.7 kbar, which also drops into the stability field of the retrograde mineral assemblage (the red circle 2 in Figure 6). Thus the sample GR14-15-7

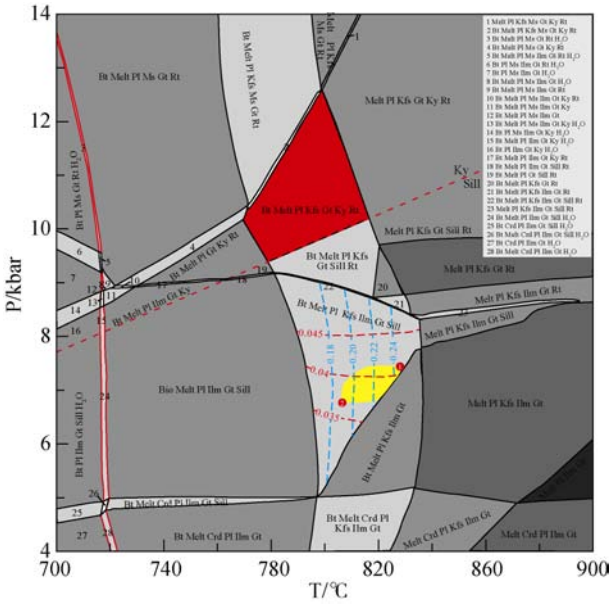

Figure 6 P-T pseudosections based on the bulk-rock compositions (SiO_2 = 73.78, TiO_2 = 0.99, Al_2O_3 = 10.01, FeO = 7.52, MgO = 1.48, MnO = 0.05, CaO = 0.85, Na_2O = 1.08, K_2O = 2.12, and H_2O = 0.96 in wt. %) of the HP pelitic granulite sample GR14-15-7 from the Grove Mountains in the MnNCKFMASHT system. The red thick line is the solidus; the red bold fonts refer to the observed peak and retrograde mineral assemblages. The blue and red dashed lines represent isopleths of X_{Mg} and X_{Ca} in garnet, respectively. The semitransparent red circles marked by numbers 1 and 2 refer to the P-T conditions constrained by the garnet composition isopleths, respectively. The red and yellow districts represent peak and retrograde metamorphic conditions, respectively.

underwent peak-stage granulite-facies metamorphism at P-T conditions of 770–815°C and 9.4–12.6 kbar, followed by a decompression of 806–828°C and 6.7–7.5 kbar.

In summary, phase equilibrium modeling shows that the

HP pelitic granulities from glacial moraines in the Grove Mountains experienced two major stages of metamorphic evolution. The peak-stage granulite-facies metamorphism P-T conditions are 817–834°C and 11.6–13.6 kbar, followed by a near-isothermal decompression of 806–828°C and 6.7–7.5 kbar.

5 Zircon trace element and U-Pb dating

Zircons of two HP pelitic granulite samples are oval to spherical in shape, with grain sizes of 50–200 μm. CL images show most grains have a small, highly luminescent inherited core with oscillatory zoning and a dark rim with diffuse zoning, the latter type also occurs as individual grains (Figure 7). Futhermore, some zircon grains have a very thin gray outer rim, probably reflecting a late stage of metamorphic growth. Excluding the inherited cores, the analyzed zircon diffuse-zoned domains of two HP pelitic granulite samples have rather high LREE content compared with HREE and display flat HREE patterns, with relatively positive Ce anomalies (Figures 8a, 8b), suggesting a metamorphic origin and growth synchronous with garnet (e.g., Rubatto et al., 2013; Rubatto and Hermann, 2007; Corfu et al., 2003; Rubatto, 2002). Zircon grains of sample GR14-3-18 have low REE contents of 15–95 ppm and slightly positive Eu anomalies. The dark and grew zircons have similar REE content and REE pattern. Zircon grains of sample GR14-15-7 have higher REE contents of 55–257 ppm and partially analyzed spots have negative Eu anomalies.

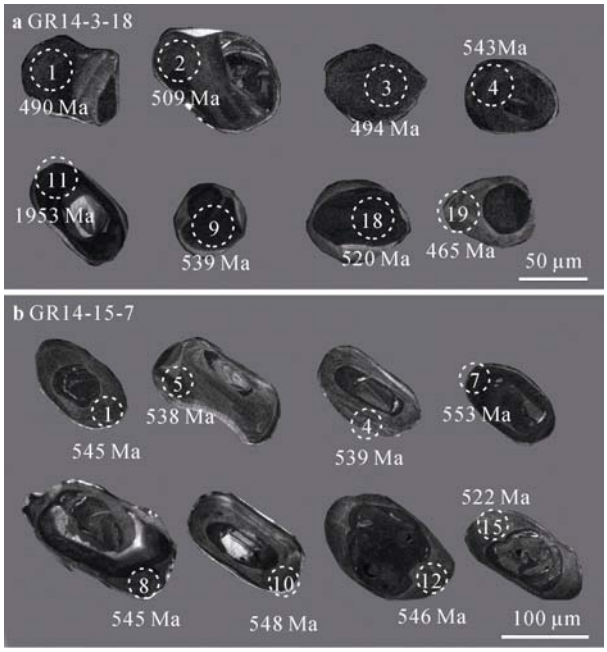

Figure 7 Representative cathodoluminescence (CL) images of zircon from HP pelitic granulites from the Grove Mountains. **a**, Zircons from sample GR14-3-18; **b**, Zircons from sample GR14-15-7. Circles with numbers are analytical spots with their identification numbers.

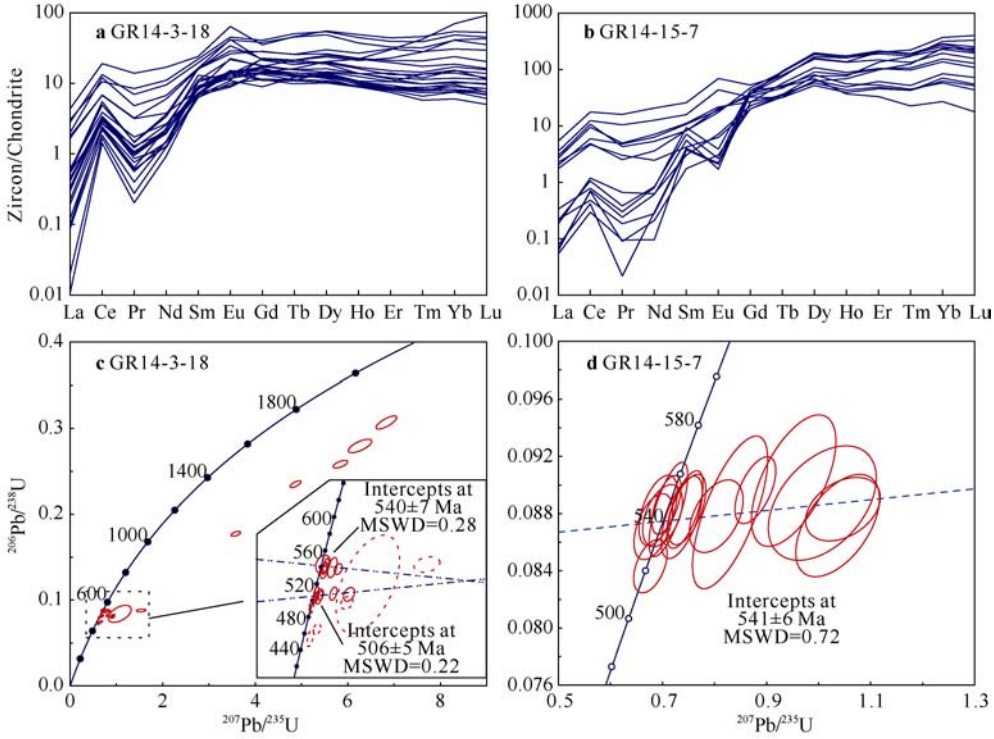

Figure 8 Chondrite-normalized REE patterns of zircon and concordia diagrams of LA-ICP-MS zircon U-Pb dating from HP pelitic granulite from the Grove Mountains. **a**, Chondrite-normalized REE patterns of zircon from sample GR14-3-18; **b**, Chondrite-normalized REE patterns of zircon from sample GR14-15-7; **c**, Concordia diagram for sample GR14-3-18; **d**, Concordia diagram for sample GR14-15-7.

For sample GR14-3-18, twenty-four spot analyses on 24 zircon diffuse zoning domains show U abundances of 399–1690 ppm and Th abundances of 10–31 ppm; with Th/U ratios <0.1. Among them, five spot analyses on 5 zircons with oscillatory-zoned cores show strong radiogenic Pb loss, and gave $^{207}Pb/^{206}Pb$ ages ranging from 2488 ± 23 Ma to 2025 ± 62 Ma, which may represent geologically meaningless mixed ages. There is no regular variation in $^{206}Pb/^{238}U$ age between the other dark and gray zircon diffuse zoning domains. Except for two discordant spots (18, 20) and three young spots (17, 19, and 21), the 7 dark domains yield a weighted mean age of 540 ± 4 Ma (MSWD=0.28) and an intercept age of 540 ± 7 Ma (MSWD=0.28), and the other 7 grey domains yield a weighted mean age of 506 ± 4 Ma (MSWD=0.20) and an intercept age of 506 ± 5 Ma (MSWD=0.22) (Figure 8c).

For sample GR14-15-7, fifteen spot analyses on 15 zircon diffuse zoning domains show U abundances of 399–1690 ppm and Th abundances of 10–31 ppm; with Th/U ratios <0.1. The $^{206}Pb/^{238}U$ ages range between 553 ± 9 Ma and 522 ± 7 Ma. All fifteen analyses give a weighted mean age of 542 ± 5 Ma (MSWD=0.75) and an intercept age of 541 ± 6 Ma (MSWD=0.72) (Figure 8d).

6 Discussion

6.1 Provenance of HP pelitic granulites

The glacial moraines from the Grove Mountains have come in many sizes, from several meters to 5 cm. Most of them show evidence of wind erosion and have sub-rounded shapes. However, the HP granulites from the glacial moraines are commonly medium-rounded with a size of 10–30 cm, suggesting a certain distance of glacial transport (Hu et al., 2016; Wang et al., 2016a, 2016b; Liu et al., 2009b). Topographically, the Grove Mountains area is subglacial highlands of about 200 km × 300 km, separated from the Gamburtsev Subglacial Mountains by a deep ice valley in the south, and bounded by a large subglacial basin to the east (Lythe et al., 2001). Remote sensing imaging and field observation suggest that the ice in the Grove Mountains flows towards the Lambert Glacier, in a predominantly NW direction of 280°–300°. Therefore, the glacial moraines from the Grove Mountains should come from the bedrocks of the nunataks or the southeastern subglacial bedrocks in the Grove Mountains.

The glacial moraines from the Grove Mountains consist mainly of high-grade metamorphic rocks and granitoids. Except for HP mafic-pelitic granulites, almost all glacial moraines could be found on the bedrock exposures of the nunataks. At the same time, geochronological studies suggest that zircon U-Pb dating of the sand- to gravel-grade clasts in the moraines is very similar to those from the bedrock exposures of the nunataks (Wang et al., 2016a, 2016b; Hu et al., 2015). This suggests that most moraine erratics from the Grove Mountains may have been accumulated nearly *in situ*, only a small fraction of glacial moraines (such as the HP mafic-pelitic granulites) may be from the subglacial bedrock in the Grove Mountains. Although the depositional age of the HP pelitic granulites was not obtained, they also underwent a 570–500 Ma high-grade metamorphic event, comparable to that of the HP mafic granulites (Liu et al., 2009b). Therefore, we infer that the HP pelitic granulites should be from the subglacial bedrock in the Grove Mountains and important components of the Pan-Afrian Prydz Belt.

6.2 P-T-t path of HP pelitic granulites

The mineral textures and phase equilibrium relations suggest that HP pelitic granulites from the Grove Mountains experienced two major stages of metamorphic evolution. The peak HP granulite facies assemblage consists of garnet + kyanite + K-feldspar + biotite + plagioclase + quartz + rutile. Garnet compositional isopleths give peak P-T estimates of 817–834°C and 11.6–13.6 kbar in the Grt–Bt–Ky–Kfs–Pl–Qz–Rt–melt field of the MnNCKFMASHT system. The post-peak decompression assemblage is represented by sillimanite replacing kyanite and biotite + sillimanite + plagioclase symplectite. The compositional isopleths of garnet rims constrain P–T conditions of 806–828°C and 7.8–8.3 kbar in the Grt–Bt–Sil–Kfs–Pl–Qz–ilm-melt fields. Taken together, the mineral assemblages and their P–T conditions constrained by the pseudosection analysis define a clockwise P-T path involving near-isothermal decompression (ITD) for the HP pelitic granulites from the Grove Mountains. The inclusion patterns of zoned garnet cores in two samples may suggest a pressure and temperature increasing process before arriving at metamorphic peak stage. However, the garnet cores and mantles do not show a pronounced compositional variation, indicating a compositional homogenization at the peak metamorphic stage. Therefore, existing metamorphic evidences is insufficient to establish a complete P-T-t path for the pelitic granulites, especially the prograde metamorphic P-T paths, and further study is still needed for detailed petrogenetic processes or burial history of the HP pelitic granulites. For HP mafic granulites from the Grove Mountains, the metamorphic textural development and P-T evolution are comparable. The metamorphic peak assemblages are dominated by garnet + clinopyroxene + hornblende + plagioclase + quartz + rutile, with relatively high X_{Grs} and X_{Prp} in garnet, slightly high Na_2O and Al_2O_3 contents in clinopyroxene and low X_{An} in plagioclase, with peak conditions of 11.8–14.0 kbar, 770–840°C (Liu et al., 2009b, 2013). The imprinted MP granulite facies metamorphism (7.0–8.5 kbar, 740–770°C), is character-rized by corona of orthopyroxene and plagioclase around garnet, and exsolution of orthopyroxene and hornblende lamellae from clinopyroxene, defining a near-isothermal decompression (ITD) P-T path (Figure 9).

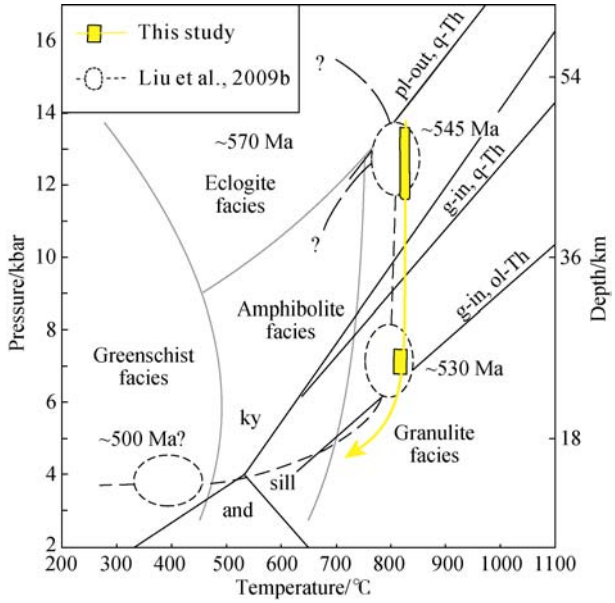

Figure 9 Metamorphic P-T evolution of HP granulites from the Grove Mountains. P-T path of HP mafic granulites (gray line) is after Liu et al. (2009b).

The dated metamorphic zircons from the two HP pelitic granulites show weak regular zoning and have low HREE contents and flat or even depleted HREE patterns, and very low Th/U ratios (<0.1; Table 3). These features are of typical metamorphic zircon that grew coevally with garnet during granulite-facies metamorphism and associated partial melting (Rubatto et al., 2013; Harley et al., 2007; Rubatto and Hermann, 2007; Corfu et al., 2003; Rubatto, 2002). These zircon grains gave metamorphic ages of 540 ± 4 Ma (sample GR14-3-18) and 542 ± 5 Ma (sample GR14-15-7), which are in agreement with peak metamorphic ages (542–545 Ma) obtained from the HP mafic granulites in the Grove Mountains (Wang et al., 2016a, 2016b; Liu et al., 2009b). Moreover, the zircon with anorthite inclusions ages of *ca*. 530 Ma and Sm-Nd garnet-whole-rock ages of 538–533 Ma were obtained for the HP mafic granulites, reflecting the time of retrograde metamorphism (Wang et al., 2016a, 2016b; Liu et al., 2009b). We propose, therefore, that the 540–545 Ma and *ca*. 530 Ma ages respectively represent the time of metamorphic peak and MP granulite facies retrograde metamorphism, for the HP pelitic granulites in the Grove Mountains. Regionally, the deformation ages of large-scale low-angle ductile shear zone developed in the Grove Mountains are determined to be *ca*. 510–490 Ma using $^{40}Ar/^{39}Ar$ dating of hornblende and biotite (Hu et al., 2015), whereas the emplacement ages of granites and granitic dykes are also concentrated at *ca*. 500 Ma (Liu et al., 2006; Zhao et al., 2003). It is likely that the young age of *ca*. 506 Ma obtained for sample GR14-3-18 is a response to late large-scale ductile shear developed in the Grove Mountains.

6.3 Tectonic implication for the Grove Mountains

The Grove Mountains are an inland continuation of the Prydz Belt in East Antarctica (Liu et al., 2009b, 2007b, 2006; Zhao et al., 2003, 2000; Mikhalsky et al., 2001a). The Prydz Belt is considered to be a Pan-African continent–continent collisional belt between the Indo-Antarctic and Australo-Antarctic continental blocks (e.g., Grew et al., 2012; Boger, 2011; Kelsey et al., 2008; Meert and Lieberman, 2008; Liu et al., 2007a, 2007b; Collins and Pisarevsky, 2005; Fitzsimons, 2003, 2000; Zhao et al., 2003, 2000; Boger et al., 2001; Hensen and Zhou, 1997). Such a tectonic model is strongly supported by the fact that all the basement and cover sequences of the Prydz Belt have suffered from the same Pan-African high-grade metamorphism and showed the same clockwise metamorphic P-T paths (Carson et al., 1997; Fitzsimons, 1996; Thost et al., 1994, 1991). However, the high-grade rocks, as petrological evidence for the tectonic nature of the Prydz belt, were metamorphosed under low- to medium-pressure granulite facies conditions with relics of the Grenvillian high-grade metamorphim (e.g., Tong et al., 2014; Liu et al., 2009a, 2007a; Wang et al., 2008; Hensen and Zhou, 1995; Ren et al., 1992). Hence some researchers consider that the Prydz Belt is an intraplate reworking belt that developed in response to the collision between East and West Gondwana or to convergent orogeny along the proto-Pacific margin of Gondwana (e.g., Tong et al., 2017, 2014, 2002, 1998; Mikhalsky et al., 2013, 2010; Halpin et al., 2012; Wang et al., 2008; Wilson et al., 2007; Phillips et al., 2006; Yoshida et al., 2003; Wilson et al., 1997; Yoshida, 1995). The absence of evidence for pre-collisional oceanic closure and subduction in the Prydz Belt seems to support this assumption. Liu et al. (2009b) identified a number of Pan-African HP mafic granulites from the glacial moraines in the Grove Mountains, which provide fundamental evidence for a collisional tectonic setting of the Prydz Belt. Wang et al. (2016b) reported that the HP mafic granulites were widely distributed in glacial moraines from the Grove Mountains. Whereas HP pelitic granulites, which are regarded as a hallmark of continental subduction and collision tectonics (e.g., O'Brien and Rotzler, 2003), have not been recognized in the Prydz Belt until this study.

In this paper, we have for the first time reported the presence of HP pelitic granulites from the Grove Mountains in the inland segment of the Prydz Belt. The discovered HP pelitic granulites contain evidence of the peak HP assemblage of garnet + kyanite + K-feldspar + biotite + plagioclase + quartz + rutile; and the post-peak decompressional assemblages as indicated by sillimanite replacing kyanite, the formation of the biotite + sillimanite symplectite in the matrix. These mineral assemblages and their P-T conditions in conjunction with the zircon U-Pb ages suggest that HP metamorphism with metamorphic peak of 11.6–13.6 kbar at 817–834°C followed by a near-isothermal decompression of 6.7–7.5 kbar at 806–

828°C might have occurred in the Grove Mountains during the Pan-African period. Such a clockwise P-T-t path is compared with that of the HP mafic granulites in the Grove Mountains and the metasediments and metabasites in the southern PCM, reflecting tectonic processes with initial crustal thickening and subsequently rapid exhumation (Gulbin et al., 2016; Liu et al., 2009b). Therefore, the development of the Prydz Belt must have been involved in continental subduction and/or collision because only subduction and collision could bring the sedimentary precursors of pelitic granulites to such a great crustal depth where they experienced HP granulite-facies metamorphism. In fact, the geochronology and geochemistry suggest that 547–497 Ma syn-orogenic charnockites and post-orogenic A-granites are widespread in the Prydz Belt (Liu et al., 2009a, 2007b, 2006; Wang et al., 2008; Li et al., 2007; Zhao et al., 2003, 2000, 1992; Carson et al., 1996). Therefore, the HP pelitic granulites reported in this study and the reconstructed P-T-t path further support the proposed tectonic model that the Prydz Belt represents a Pan-African continent–continent collisional belt between the Indo-Antarctic and Australo-Antarctic continental blocks (Liu et al., 2013, 2009a, 2009b, 2007a, 2007b, 2006; Grew et al., 2012; Boger, 2011; Kelsey et al., 2008; Meert and Lieberman, 2008; Collins and Pisarevsky, 2005; Fitzsimons, 2003; 2000; Harley, 2003; Zhao et al., 2003; Boger et al., 2001; Hensen and Zhou, 1997).

7 Conclusions

Based on detailed metamorphic petrological and geochronological studies for the HP pelitic granulites from glacial moraines of the Grove Mountains in the Prydz Belt, we conclude the following:

(1) Petrographic evidence and phase equilibrium modelling for HP pelitic granulites define the peak P-T conditions at 817–834°C and 11.6–13.6 kbar, and a clockwise near-isothermal decompression P-T path.

(2) Zircon U-Pb dating constrains the HP granulite facies metamorphism to have occurred at *ca*. 540 Ma in the Grove Mountains, which is an island continuation of the Pan-African Prydz Belt.

(3) The firstly recognized Pan-Afrian HP pelitic granulites from the glacial moraines of the Grove Mountains provide new petrological evidence for a collisional tectonic setting of the Pan-Afrian Prydz Belt.

Acknowledgments We would like to thank Zhao Junmeng, Liu Hongbing, Li Jinyan, Li Yawei, Yang Wenqing, Miao Bingkui, Yao Xu, and Fei Yuhao for assistance during fieldwork. Thorough and constructive reviews by L. Tong, E. V. Mikhalsky and N. Alexeev substantially improved the manuscript. Field work was carried out during the 2013/2014 Chinese National Antarctic Research Expedition. We gratefully acknowledge logistical support from the Chinese Arctic and Antarctic Administration, SOA, and financial support from the National Natural Science Foundation of China (Grant no. 41530209), the Central Public-Interest Scientific Institution Basal Research Fund (Grant no. JYYWF201819), the Chinese Polar Environment Comprehensive Investigation & Assessment Programs (Grant no. CHINARE2015-02-05), and the Geological Investigation Project of the China Geological Survey (Grant no. 12120113019000).

References

Anderson J R, Payne J L, Kelsey D E, et al. 2012. High-pressure granulites at the dawn of the Proterozoic. Geology, 40(5): 431-434.

Appel P, Schenk V. 1998. High-pressure granulite facies metamorphism in the Pan–African belt of eastern Tanzania: P-T-t evidence against granulite formation by continent collision. J Metamorph Geol, 16(4): 491-509.

Beliatsky B V, Laiba A A, Mikhalsky E V. 1994. U-Pb zircon age of the metavolcanic rocks of Fisher Massif (Prince Charles Mountains, East Antarctica). Antarct Sci, 6(3): 355-358.

Benisek A, Dachs E, Kroll H. 2010. A ternary feldspar–mixing model based on calorimetric data: development and application. Contrib Mineral Petrol, 160(3): 327-337.

Boger S D. 2011. Antarctica–before and after Gondwana. Gondwana Res, 19: 335-371.

Boger S D, Carson C J, Fanning C M, et al. 2002. Pan–African intraplate deformation in the northern Prince Charles Mountains, East Antarctica. Earth Planet Sci Lett, 195(3-4): 195-210.

Boger S D, Carson C J, Wilson C J L, et al. 2000. Neoproterozoic deformation in the Radok Lake region of the northern Prince Charles Mountains, East Antarctica; evidence for a single protracted orogenic event. Precambrian Res, 104(1): 1-24.

Boger S D, Wilson C J L. 2005. Early Cambrian crustal shortening and a clockwise P-T-t path from the southern Prince Charles Mountains, East Antarctica: implications for the formation of Gondwana. J Metamorph Geol, 23(7): 603-623.

Boger S D, Wilson C J L, Fanning C M. 2001. Early Paleozoic tectonism within the East Antarctic craton: the final suture between east and west Gondwana? Geology, 29(5): 463-466.

Carson C J, Boger S D, Fanning C M, et al. 2000. SHRIMP U-Pb geochronology from Mount Kirkby, northern Prince Charles Mountains, East Antarctica. Antarct Sci, 12: 429-442.

Carson C J, Dirks P G H M, Hand M, et al. 1995. Compressional and extensional tectonics in low–medium pressure granulites from the Larsemann Hills, East Antarctica. Geol Mag, 132: 151-170.

Carson C J, Fanning C M, Wilson C J L. 1996. Timing of the progress granite. Larsemann Hills: Additional evidence for Early Palaeozoic orogenesis within the East Antarctica Shield and implications for Gondwana assembly. Aust J Earth Sci, 43: 539-553.

Carson C J, Powell P, Wilson C J L, et al. 1997. Partial melting during tectonic exhumation of a granulite terrane: an example from the Larsemann Hills, East Antarctica. J Metamorph Geol, 15: 105-126.

Coggon R, Holland T J B. 2002. Mixing properties of phengitic micas and revised garnet–phengite thermobarometers. J Metamorph Geol, 20: 683-696.

Collins A S, Pisarevsky S A. 2005. Amalgamating eastern Gondwana: the evolution of the Circum–Indian Orogens. Earth Sci Rev, 71: 229-270.

Connolly J A D. 2005. Computation of phase equilibria by linear

programming: a tool for geodynamic modeing and its application to subduction zone decarbonation. Earth Planet Sci Lett, 236: 524-541.

Corfu F, Hanchar J M, Hoskin P W, et al. 2003. Atlas of zircon textures. Rev Mineral Geochem, 53: 469-500.

Dalziel I W D. 1991. Pacific margins of Laurentia and East Antarctica–Australia as a conjugate rift pair: evidence and implications for an Eocambrian supercontinent. Geology, 19: 598-601.

Dirks P H G M, Wilson C J L. 1995. Crustal evolution of the East Antarctic mobile belt in Prydz Bay: continental collision at 500 Ma? Precambrian Res, 75: 189-207.

Fitzsimons I C W. 2003. Proterozoic basement provinces of southern and southwestern Australia, and their correlation with Antarctica. J Geol Soc London, Spec Publ, 206: 93-130.

Fitzsimons I C W. 2000. Grenville–age basement provinces in East Antarctica: evidence for three separate collisional orogens. Geology, 28: 879-882.

Fitzsimons I C W. 1997. The Brattstrand Paragneiss and the Søstrene Orthogneiss: a review of Pan–African metamorphism and Grenvillian relics in southern Prydz Bay//Ricci C A. The Antarctic Region: Geological Evolution and Processes. Terra Antarct Publ, Siena, 121-130.

Fitzsimons I C W. 1996. Metapelitic migmatites from Brattstrand Bluffs, East Antarctica–metamorphism, melting and exhumation of the mid crust. J Petrol, 37: 395-414.

Fitzsimons I C W, Harley S L. 1991. Geological relationships in high-grade gneisses of the Brattstrand Bluffs coastline, Prydz Bay, East Antarctica. Aust J Earth Sci, 38: 497-519.

Grew E S, Carson C J, Christy A G, et al. 2012. New constraints from U-Pb, Lu-Hf and Sm-Nd isotopic data on the timing of sedimentation and felsic magmatism in the Larsemann Hills, Prydz Bay, East Antarctica. Precambrian Res, 206-207: 87-108.

Grew E S, Manton W I. 1981. Geochronologic studies in East Antarctica: ages of rocks at Reinbolt Hills and Molodezhnaya Station. Antarc J United States,16: 5-7.

Gulbin Y L, Egorova K V, Mikhalsky E V, et al. 2016. New data on the metamorphism of the Neoproterozoic Sodruzhestvo Group in southern Prince Charles Mountains, East Antarctica. The 35th International Geological Congress.

Halpin J A, Daczko N R, Milan L A, et al. 2012. Decoding near-concordant U-Pb zircon ages spanning several hundred million years: recrystallisation, metamictisation or diffusion? Contrib Mineral Petrol, 163(1): 67-85.

Harley S L. 2003. Archaean–Cambrian crustal development of East Antarctica: metamorphic characteristics and tectonic implications// Yoshida M, Windley B, Dasgupta S. Proterozoic East Gondwana: Supercontinent Assembly and Breakup. J Geol Soc London, Spec Publ, 206: 203-230.

Harley S L, Fitzsimons I C W, Zhao Y. 2013. Antarctica and supercontinent evolution: historical perspectives, recent advances and unresolved issues. J Geol Soc London, Spec Publ, 383: 1-34.

Harley S L, Kelly N M, Möller A. 2007. Zircon behaviour and the thermal histories of Mountain Chains. Elements, 3: 25-30.

Harley S L, Snape I, Black L P. 1998. The early evolution of a layered metaigneous complex in the Rauer Group, East Antarctica: evidence for a distinct Archaean terrane. Precambrian Res, 89: 175-205.

Hensen B J, Zhou B. 1995. A Pan–African granulite facies metamorphic episode in Prydz Bay, Antarctica: Evidence from Sm-Nd garnet dating. Aust J Earth Sci, 42: 249-258.

Hoffman P F. 1991. Did the breakout of Laurentia turn Gondwanaland inside out? Science, 252: 1409-1412.

Holdway M J, Mukhopadhyay B, Dyar M D, et al. 1997. Garnet–biotite geothermometry revised: new Margules parameters and a natural specimen data set from Maine. Am Mineral, 82: 582-595.

Holland T J B, Powell R. 1998. An internally consistent thermodynamic data set for phases of petrological interest. J Metamorph Geol, 16: 309-343.

Hu J M, Ren M H, Zhao Y, et al. 2016. Source region analyses of the morainal detritus from the Grove Mountains: Evidence from the subglacial geology of the Ediacaran–Cambrian Prydz Belt of East Antarctica. Gondwana Res, 35: 164-179.

Hu Z C, Liu Y S, Gao S, et al. 2008. A local aerosol extraction strategy for the determination of the aerosol composition in Laser Ablation Inductively Coupled Plasma Mass Spectrometry, J Anal Atom Spectrom, 23: 1192-1203.

Indares A D, White R W, Powell R. 2008. Phase equilibria modelling of kyanite–bearing anatectic paragneisses from the central Grenville Province. J Metamorph Geol, 26: 815-836.

Kelsey D E, Hand M, Clark C, et al. 2007. On the application of *in situ* monazite chemical geochronology to constraining P-T-t histories in high–temperature (>850°C) polymetamorphic granulites from Prydz Bay, East Antarctica. J Geol Soc London, 164(3): 667-683.

Kelsey D E, Powell R, Wilson C J L, et al. 2003. (Th+U)-Pb monazite ages from Al-Mg-rich metapelites, Rauer Group, East Antarctica. Contrib Mineral Petrol, 146: 326-340.

Kelsey D E, Wade B P, Collins A S, et al. 2008. Discovery of a Neoproterozoic basin in the Prydz belt in East Antarctica and its implications for Gondwana assembly and ultrahigh temperature metamorphism. Precambrian Res, 161(3): 355-388.

Kinny P D, Black L P, Sheraton J W. 1997. Zircon U-Pb ages and geochemistry of igneous and metamorphic rocks in the northern Prince Charles Mountains, Antarctica. AGSO J Aust Geol Geophys, 16(5): 637-654.

Kinny P D, Black L P, Sheraton J W. 1993. Zircon ages and the distribution of Archean and Proterozoic rocks in the Rauer Islands. Antarct Sci, 5(2): 193-206.

Li M, Liu X C, Zhao Y. 2007. Zircon U-Pb ages and geochemistry of granitoids from Prydz Bay, East Antarctica, and their tectonic significance. Acta Petrol Sin, 23(5): 1055-1066 (in Chinese with English abstract).

Liu X C, Jahn B M, Zhao Y, et al. 2014a. Geochemistry and geochronology of Mesoproterozoic basement rocks from the eastern Amery Ice Shelf and southwestern Prydz Bay, East Antarctica: Implications for a long-lived magmatic accretion in a continental arc. Am J Sci, 314 (2): 508-547.

Liu X C, Wang W, Zhao Y, et al. 2014b. Early Neoproterozoic granulite facies metamorphism of mafic dykes from the Vestfold Block, East Antarctica. J Metamorph Geol, 32 (9): 1041-1062.

Liu X C, Jahn B M, Zhao Y, et al. 2006. Late Pan-African granitoids from the Grove Mountains, East Antarctica: age, origin and tectonic implications. Precambrian Res, 145(1): 131-154.

Liu X C, Zhao Y, Zhao G, et al. 2007a. Petrology and geochronology of granulites from the McKaskle Hills, eastern Amery Ice Shelf,

Antarctica, and implications for the evolution of the Prydz Belt. J Petrol, 48(8): 1443-1470.

Liu X C, Jahn B M, Zhao Y, et al. 2007b. Geochemistry and geochronology of high grade rocks from the Grove Mountains, East Antarctica: evidence for an Early Neoproterozoic basement metamorphosed during a single Late Neoproterozoic/Cambrian tectonic cycle. Precambrian Res, 158(1): 93-118.

Liu X C, Zhao Y, Chen H, et al. 2017. New zircon U-Pb and Hf-Nd isotopic constraints on the timing of magmatism, sedimentation and metamorphism in the northern Prince Charles Mountains, East Antarctica. Precambrian Res, 299: 15-33.

Liu X C, Zhao Y, Hu J M. 2013. The *ca*. 1000–900 Ma and *ca*. 550–500 Ma tectonothermal events in the Prince Charles Mountains–Prydz Bay region, East Antarctica, and their relations to supercontinent evolution//Harley S L, Fitzsimons I C W, Zhao Y. Antarctica and Supercontinent Evolution. J Geol Soc London, Spec Publ, 283: 95-112.

Liu X H, Zhao Y, Liu X C, et al. 2003. Geology of the Grove Mountains in East Antarctica—new evidence for the final suture of Gondwana Land. Sci China (Ser D), 46(4): 305-319.

Liu X C, Zhao Y, Liu X H. 2002. Geological aspects of the Grove Mountains, East Antarctica//Gamble J A, Skinner D N B, Henrys S. Antarctica at the close of a Millennium. R Soc New Zealand Bull, 35: 161-166.

Liu X C, Zhao Y, Song B, et al. 2009a. SHRIMP U-Pb zircon geochronology of high-grade rocks and charnockites from the eastern Amery Ice Shelf and southwestern Prydz Bay, East Antarctica: constraints on Late Mesoproterozoic to Cambrian tectonothermal events related to Supercontinent Assembly. Gondwana Res, 16(2): 342-361.

Liu X C, Hu J M, Zhao Y, et al. 2009b. Late Neoproterozoic/Cambrian high–pressure mafic granulites from the Grove Mountains, East Antarctica: P-T-t path, collisional orogeny and implications for assembly of Gondwana. Precambrian Res, 174(1): 181-199.

Liu Y S, Gao S, Hu Z C, et al. 2010. Continental and oceanic crust recycling–induced melt–peridotite interactions in the Trans–North China Orogen: U-Pb dating, Hf isotopes and trace elements in zircons of mantle xenoliths. J Petrol, 51(1-2): 537-571.

Ludwig K R. 2003. User's manual for Isoplot 3.00: a geochronological toolkit for Microsoft Excel.

Lythe M B, Vaughan D G, the BEDMAP Consortium, 2001. BEDMAP: a new ice thickness and subglacial topographic model of Antarctica. J Geophys Res, 106 (B6): 11335-11351.

Manton W I, Grew E S, Hofmann J, et al. 1992. Granitic rocks of the Jetty Peninsula, Amery Ice Shelf area, East Antarctica//Yoshida Y, Kaminuma K, Shiraishi K. Recent progress in Antarctic Earth Science, Terra Scientific Publishing Company, Tokyo, 179-189.

Mcdonough W F, Sun S S. 1995. The composition of the Earth. Chem Geol, 120 (3-4): 223-253.

Meert J G, Lieberman B S. 2008. The Neoproterozoic assembly of Gondwana and its relationship to the Ediacaran–Cambrian radiation. Gondwana Res. 14(1), 5-21.

Mikhalsky E V, Henjes-Kunst F, Belyatsky B V, et al. 2010. New Sm–Nd, Rb–Sr, U–Pb and Hf isotope systematics for the southern Prince Charles Mountains (East Antarctica) and its tectonic implications. Precambrian Res, 182(1): 101-123.

Mikhalsky E V, Kamenev I A. 2013. Recurrent transitional group charnockites in the east Amery Ice Shelf coast (East Antarctica): Petrogenesis and implications on tectonic evolution. Lithos, 175-176(3): 230-243.

Mikhalsky E V, Laiba A A, Beliatsky B V, et al. 1999. Geology, age and origin of the Mount Willing area (Prince Charles Mountains, East Antarctica). Antarct Sci, 11(3): 338-352.

Mikhalsky E V, Sheraton J W, Beliatsky B V. 2001a. Preliminary U–Pb dating of Grove Mountains rocks: implications for the Proterozoic to Early Palaeozoic tectonic evolution of the Lambert Glacier–Prydz Bay area (East Antarctica). Terra Antart, 8(1): 3-10.

Mikhalsky E V, Sheraton J W, Laiba A A, et al. 2001b. Geology of the Prince Charles Mountains, Antarctica. AGSO–Geoscience Australia Bulletin, 247.

Moores E M. 1991. Southwest U.S.−East Antarctic (SWEAT) connection: a hypothesis. Geology, 19: 425-428.

Morrissey L J, Hand M, Kelsey D E, et al. 2016. Cambrian high–temperature reworking of the Rayner–Eastern Ghats Terrane: constraints from the northern Prince Charles Mountains region, East Antarctica. J Petrol, 57: 53-92.

Morrissey L J, Hand M, Kelsey D E. 2015. Multi-stage metamorphism in the Rayner–Eastern Ghats Terrane: P-T-t constraints from the northern Prince Charles Mountains, East Antarctica. Precambrian Res, 267: 137-163.

Pearce N J G, Perkins W T, Westgate J A, et al. 1996. A compilation of new and published major and trace element data for NIST SRM 610 and NIST SRM 612 glass reference materials. Geostandard Newslett, 21: 115-144.

Phillips G, White R W, Wilson C J L. 2007. On the role of deformation and fluid during rejuvenation of a polymetamorphic terrane: inferences on the geodynamic evolution of the Ruker Province, East Antarctica. J Metamorph Geol, 25(8): 855-871.

Phillips G, Wilson C J L, Campbell I H, et al. 2006. U–Th–Pb detrital zircon geochronology from the southern Prince Charles Mountains, East Antarctica–defining the Archaean to Neoproterozoic Ruker Province. Precambrian Res, 148(3-4): 292-306.

Ren L D, Zhao Y, Liu X C, et al. 1992. Re-examination of the metamorphic evolution of the Larsemann Hills, East Antarctica//Yoshida Y. Recent progress in Antarctic Earth Science. Terra Scientific Publishing, Tokyo, 145-153.

Rubatto D. 2002. Zircon trace element geochemistry: partitioning with garnet and the link between U–Pb ages and metamorphism. Chem Geol, 184(1): 123-138.

Rubatto D, Chakraborty S, Dasgupta S. 2013. Timescales of crustal melting in the Higher Himalayan Crystallines (Sikkim, Eastern Himalaya) inferred from trace element constrained monazite and zircon chronology. Contrib Mineral Petrol, 165(2): 349-372.

Rubatto D, Hermann J. 2007. Zircon behaviour in deeply subducted rocks. Elements, 3(1): 31-35.

Sheraton J W, Black L P, Mcculloch M T. 1984. Regional geochemical and isotopic characteristics of high-grade metamorphics of the Prydz Bay area: The extent of Proterozoic reworking of Qrchaean continental crust in East Antarctica. Precambrian Res, 26(2): 169-198.

Stern R J. 1994 Arc-assembly and continental collision in the Neoproterozoic African orogen: implications for the consolidation of Gondwanaland. Annu Rev Earth Planet Sci, 22(1): 319-351.

Tajčmanová L, Connolly J, Cesare B. 2009. A thermodynamic model for

titanium and ferric iron solution in biotite. J Metamorph Geol, 27(2): 153-165.

Thost D E, Hensen B J, Motoyoshi Y. 1994. The geology of a rapidly uplifted medium and low pressure granulite facies terrane of Pan African age: the Bolingen Islands, Prydz Bay, East Antarctica. Petrology, 2(4): 293-316.

Thost D E, Hensen B J, Motoyoshi Y. 1991. Two-stage decompression in garnetbearing mafic granulites from Søtrene Island, Prydz Bay, East Antarctica. J Metamorph Geol, 9(3): 245-256.

Tong L, Jahn B M, Liu X H, et al. 2017. Ultramafic to mafic granulites from the Larsemann Hills, East Antarctica: Geochemistry and tectonic implications. Journal of Asian Earth Sciences, 145(SI): 679-690.

Tong L, Liu X H, Wang Y B, et al. 2014. Metamorphic P-T paths of metapelitic granulites from the Larsemann Hills, East Antarctica. Lithos, 192-195(4): 102-115.

Tong L, Liu X H, Zhang L S, et al. 1998. The ^{40}Ar-^{39}Ar ages of hornblendes in Grt-Pl-bearing amphibolite from the Larsemann Hills, East Antarctica and their geological implications. Chin J Polar Sci, 9(2): 79-91.

Tong L, Wilson C J L. 2006. Tectonothermal evolution of the ultrahigh temperature metapelites in the Rauer Group, East Antarctica. Precambrian Res. 149(1-2): 1-20.

Tong L, Wilson C J L, Liu X H. 2002. A high-grade event of ~1100 Ma preserved within the ~500 Ma mobile belt of the Larsemann Hills, East Antarctica: further evidence from ^{40}Ar-^{39}Ar dating. Terra Antart, 9: 73-86.

Wang W, Liu X C, Zhao Y, et al. 2016a. U-Pb zircon ages and Hf isotopic compositions of metasedimentary rocks from the Grove Subglacial Highlands, East Antarctica: Constraints on the provenance of protoliths and timing of sedimentation and metamorphism. Precambrian Res, 275: 135-150.

Wang W, Liu X C, Zhao Y, et al. 2016b. U-Pb zircon chronology of high-pressure granulites and orthogneisses from glacial moraines in the Grove Mountains, East Antarctica. Chin J Polar Res, 28(2): 159-180 (in Chinese with English abstract).

Wang Y B, Liu D Y, Chung S L, et al. 2008. SHRIMP zircon age constraints from the Larsemann Hills region, Prydz Bay, for a Late Mesoproterozoic to Early Neoproterozoic tectono-thermal event in East Antarctica. Am J Sci, 308(4): 573-617.

Wang Y B, Tong L X, Liu D Y. 2007. Zircon U-Pb ages from an ultra-high temperature metapelite, Rauer Group, East Antarctica: Implications for overprints by Grenvillian and Pan-African events in Antarctica: A keystone in a changing world//Cooper A K, Raymond C R et al. Online Proceedings of the 10th ISAES, USGS Open-File Report (Vol. 1047).

White R W, Powell R, Halpin A. 2004. Spatially-focused melt formation in aluminous metapelites from Broken Hill, Australia. J Metamorph Geol, 22(9): 825-845.

White R W, Powell R, Holland T J B. 2007. Progress relating to calculation of partial melting equilibria for metapelites. J Metamorph Geol, 25(5): 511-527.

White R W, Powell R, Holland T J B. 2001. Calculation of partial melting equilibria in the system Na_2O–CaO–K_2O–FeO–MgO–Al_2O_3–SiO_2–H_2O (NCKFMASH). J Metamorph Geol, 19(2): 139-153.

Wilson T J, Grunow A M, Hanson R E. 1997. Gondwana assembly: the view from southern Africa and East Gondwana. J Geodyn, 23(3-4): 263-286.

Wilson C J L, Quinn C, Tong L X, et al. 2007. Early Palaeozoic intracratonic shears and post-tectonic cooling in the Rauer Group, Prydz Bay, East Antarctica constrained by ^{40}Ar/^{39}Ar thermochronology. Antarct Sci, 19(3): 339-353.

Woodhead J, Hergt J, Shelley M, et al. 2004. Zircon Hf-isotope analysis with an excimer laser, depth profiling, ablation of complex geometries, and concomitant age estimation. Chem Geol, 209(1): 121-135.

Yoshida M. 1995. Cambrian orogenic belt in East Antarctica and Sri Lanka: implications for Gondwana assembly: a discussion. J Geol, 103(4): 467-468.

Yoshida M, Jacobs J, Santosh M, et al. 2003. Role of Pan-African events in the Circum-East Antarctic Orogen of East Gondwana: a critical overview//Yoshida M, Windley B, Dasgupta S. Proterozoic East Gondwana: Supercontinent Assembly and Breakup. Geol Soc London, Spec Publ, 206: 57-75.

Zhao Y, Liu X C, Fanning C M, et al. 2000. The Grove Mountains, a segment of a Pan-African orogenic belt in East Antarctica. Abstract Volume of the 31th IGC, Rio de Janeiro, Brazil.

Zhao Y, Liu X H, Liu X C, et al. 2003. Pan-African events in Prydz Bay, East Antarctica and its inference on East Gondwana tectonics//Yoshida M, Windley B, Dasgupta S. Proterozoic East Gondwana: Supercontinent Assembly and Breakup. J Geol Soc London, Spec Publ, 206: 231-245.

Zhao Y, Liu X H, Song B, et al. 1995. Constraints on the stratigraphic age of metasedimentary rocks from the Larsemann Hills, East Antarctica: possible implications for Neoproterozoic tectonics. Precambrian Res, 75(3-4): 175-188.

Zhao Y, Song B, Wang Y, et al. 1992. Geochronology of the late granite in the Larsemann Hills, East Antarctica//Yoshida Y, Kaminuma K, Shiraishi K. Recent progress in Antarctic Earth Science. Terra Scientific Publishing Company, Tokyo, 155-161.

Zhao Y, Song B, Wang Y B, et al. 1991. Geochronological study of the metamorphic and igneous rocks of the Larsemann Hills, East Antarctica. Proceedings of the 6th ISAES (Abstracts), Tokyo. National Institute for Polar Research, Japan, 662-663.

Zhao Y, Song B, Zhang Z, et al. 1993. An Early Palaeozoic (‘Pan African’) thermal event in the Larsemann Hills and its neighbours, Prydz Bay, East Antarctica. Sci China (Ser B), 23(9): 1001-1008 (in Chinese with English abstract).